Available online at www.sciencedirect.com
ScienceDirect
Computational Materials Science 39 (2007) 91–95
COMPUTATIONAL MATERIALS SCIENCE
www.elsevier.com/locate/commatsci

A dislocation density based constitutive law for BCC materials in crystal plasticity FEM

A. Ma, F. Roters *, D. Raabe

Abteilung Mikrostrukturphysik und Umformtechnik, Max-Planck-Institut für Eisenforschung, Max-Planck-Str. 1, 40237 Düsseldorf, Germany

Received 15 November 2005; received in revised form 15 April 2006; accepted 20 April 2006

Abstract

We introduce a crystal plasticity constitutive model for BCC materials which is build on dislocation movement and uses dislocation density variables as internal state variables. Besides the statistically stored dislocations geometrically necessary dislocations are used to consider nonlocal effects as recently proposed by Ma, Roters and Raabe for the FCC crystal structure. In this paper the model will be adopted to the BCC crystal structure. Due to the special core structure of screw dislocations formed at low temperatures, the mechanical behavior of BCC crystals is controlled by the movement of screw dislocations rather than edge dislocations. For this reason, the Peierls mechanism has to be considered and several modifications have been introduced which include a new scaling relation between the mobile and immobile dislocations, and new flow rules for bulk and grain boundary elements. A pure Nb bicrystal is studied experimentally and numerically under channel die compression boundary conditions, to demonstrate the applicability of the new model variant.

Keywords: Dislocation density; Constitutive equation; BCC; Slip system; Bulk element; Grain boundary element; Peierls mechanism

1. Introduction

For FCC crystals the calculated Peierls stress is much smaller than the measured critical resolved stress as there exist close packed lattice planes and close packed lattice directions. Therefore, it can be assumed, that the resistance for moving dislocations is determined by the passing stress and the cutting stress due the other dislocations in the crystal only. BCC single crystals, in contrast, have only densely-packed lattice directions but no densely-packed lattice planes. In the literature 24–48 slip systems are reported to be activated to accommodate the external plastic deformation [1–5]. For this structure the Peierls stress is so large that one can assume that in order to move the mobile dislocations, the external load has to overcome the resistance both, of the parallel dislocations and the Peierls energy barrier, i.e. forest cuttings can be ignored. In this paper the model introduced in [6,7] will be adopted to the BCC crystal structure.

Using the newly developed dislocation model and a digital image correlation technique [8], a pure Nb bicrystal is studied numerically and experimentally under channel die compression conditions.

2. The constitutive formulations

For the kinematic description of the plastic deformation of crystalline materials, we follow the well-known multiplicative decomposition of the deformation gradient $\mathbf{F}$ to separate the elastic and plastic portions of the deformation. The elastic part $\mathbf{F}^{e}$ comprises the stretch and rotation of the lattice, and the plastic part $\mathbf{F}^{p}$ corresponds to the unrecoverable deformation caused by dislocation slip. For the reason that the plastic deformation gradient does not change the lattice orientation, we can use a constant stiffness tensor $\mathbf{C}$ for the stress calculation. The elastic law is defined in the unloaded configuration.

* Corresponding author. Tel.: +49 211 679 2393; fax: +49 211 679 2333.
E-mail address: f.roters@mpie.de (F. Roters).

0927-0256/$ - see front matter © 2006 Elsevier B.V. All rights reserved.
doi:10.1016/j.commatsci.2006.04.014

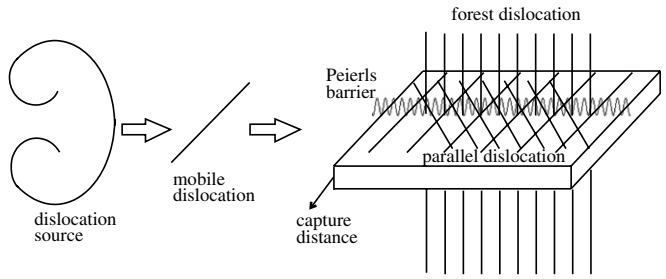

Fig. 1. Schematic drawing of the slip mechanism for the BCC crystal structure: a mobile dislocation is generated by a Frank–Read source, and the external stress must help it to overcome resistances of forest and parallel dislocations, and the Peierls energy barrier.

$$\mathbf{T} = \mathbf{C}\frac{1}{2}(\mathbf{F}^{e}\ \mathbf{F}^{e^{T}} - \mathbf{1}) \tag{1}$$

Details are given in [6].

BCC crystals have densely-packed lattice directions $\langle 1\,1\,1\rangle$ but no densely-packed lattice planes. The most densely-packed planes are the $\{1\,1\,0\}$, $\{1\,1\,2\}$ and $\{1\,2\,3\}$ lattice planes. There are at most 48 slip systems if we do not consider the so-called pencil glide. As shown in Fig. 1, the mobile dislocation experiences the slip resistance from forest and parallel dislocations, and also from the Peierls energy barrier. We define the parallel dislocation density $\rho^{\alpha}_{\mathrm{P}}$ and the forest dislocation density $\rho^{\alpha}_{\mathrm{F}}$ by the projections described in [6,9]. While in the FCC case the Peierls potential is so small that it can be neglected, it is much higher for the BCC crystal structure. In fact it is so high, that in the BCC case the forest cutting process can be neglected when formulating the dislocation velocity equation.

We are using a standard crystal plasticity finite element (CP-FEM) framework (see e.g. [10]), where the plastic velocity gradient $\mathbf{L}^{\mathrm{p}}$ can be calculated as

$$\mathbf{L}^{\mathrm{p}} = \sum_{\alpha=1}^{48} \dot{\gamma}^{\alpha}\tilde{\mathbf{d}}^{\alpha} \otimes \tilde{\mathbf{n}}^{\alpha} \tag{2}$$

where $\dot{\gamma}^{\alpha}$ is the slip rate on slip system α, $\tilde{\mathbf{d}}^{\alpha}$ expresses the slip direction, and $\tilde{\mathbf{n}}^{\alpha}$ the slip plane normal with respect to the undistorted configuration.

In contrast to [10] we are using a dislocation density based constitutive law, so that the slip rates can be calculated by use of the Orowan equation:

$$\dot{\gamma}^{\alpha} = \rho^{\alpha}_{\mathrm{M}} b v^{\alpha} \tag{3}$$

Here v^{α} is the average velocity of the mobile dislocations $\rho^{\alpha}_{\mathrm{M}}$ and b the magnitude of the respective Burgers vector. From [6,9,11] we know, that by applying the principle of maximum plastic dissipation for the external resolved shear stress during the plastic deformation

$$\frac{\partial \dot{\gamma}^{\alpha}}{\partial \rho^{\alpha}_{\mathrm{M}}} = 0 \tag{4}$$

a scaling relation can be derived for $\rho^{\alpha}_{\mathrm{M}}$. Which in the case of a homogeneous dislocation structure and for the BCC crystal structure amounts to

$$\rho^{\alpha}_{\mathrm{M}} \approx \frac{2k_{\mathrm{B}}\theta}{c_1 c_3 G b^4}\sqrt{\rho^{\alpha}_{\mathrm{P}}} \tag{5}$$

where c_1,c_3 are constants, G is the shear modulus, b the magnitude of the Burgers vector, θ the absolute temperature, and k_{B} the Boltzmann constant. One can see easily that Eq. (5) is different compared to that suggested in [6,9] for FCC materials. This is due to the fact, that the forest cutting mechanism which is assumed as the prevailing mechanism in the case of FCC crystals is replaced by the Peierls mechanism, where the jump distance amounts to the magnitude of Burgers vector b in the case of BCC.

It is a well known fact, that the classical CP-FEM is not capable of correctly describing the mechanical influence of grain boundaries. Therefore, several extension to CP-FEM are proposed to deal with grain boundaries (see e.g. [7,12]). We are following the approach used in [7] and, therefore, distinguish two different flow rules for bulk and for grain boundary elements, respectively.

2.1. Flow rule of the bulk element

Integrating (5) into (3), the flow rule is derived based on the dislocation slip mechanism. It includes a reference shear rate which is formulated as a function of the dislocation density and the temperature. The new flow rule amounts to

$$\dot{\gamma}^{\alpha} = \begin{cases} \dot{\gamma}^{\alpha}_{0}\exp\left[-\frac{Q_{\mathrm{Pei}}}{k_{\mathrm{B}}\theta}\left(1-\frac{|\tau^{\alpha}|-\tau^{\alpha}_{\mathrm{pass}}}{\tau^{\alpha}_{\mathrm{Pei}}}\right)\right]\mathrm{sign}(\tau^{\alpha}) & |\tau^{\alpha}| > \tau^{\alpha}_{\mathrm{pass}} \\ 0 & |\tau^{\alpha}| \leqslant \tau^{\alpha}_{\mathrm{pass}} \end{cases} \tag{6}$$

with the pre-exponential variable $\dot{\gamma}^{\alpha}_{0}$, which is the upper limit of the shear rate for the case that the Boltzmann factor is equal to 1 in Eq. (6)

$$\dot{\gamma}^{\alpha}_{0} = \frac{k_{\mathrm{B}}\theta v_0}{c_1 c_3 G b^2}\sqrt{\rho^{\alpha}_{\mathrm{P}}} \tag{7}$$

where γ_0 is the attack frequency and the passing stress, $\tau^{\alpha}_{\mathrm{pass}}$, caused by the parallel dislocations

$$\tau^{\alpha}_{\mathrm{pass}} = c_1 G b\sqrt{\rho^{\alpha}_{\mathrm{P}}} \tag{8}$$

and the Peierls stress, $\tau^{\alpha}_{\mathrm{Pei}}$,

$$\tau^{\alpha}_{\mathrm{Pei}} = \frac{Q_{\mathrm{Pei}}}{c_3 b^3} \tag{9}$$

where Q_{Pei} is the effective activation energy for the Peierls mechanism.

2.2. Flow rule of the grain boundary element

In general, in CP-FEM implementations the grain boundaries coincide with element boundaries. In contrast to this conventional approach we use a special grain boundary element, where one half of the Gauss points belong to one crystal, while the others belong to the abutting crystal, see details in [7,13]. For the constitutive law of material points belonging to this element class, we use a modified

flow rule where we introduce an effective activation energy for the slip process which is based on a conservation law for the Burgers vector during the slip penetration through a grain boundary. Based on Eq. (6) for the BCC crystal structure we modify $\tau^{\alpha}_{\mathrm{Pei}}$ and Q_{Pei} as follows:

$$Q_{\mathrm{eff}} = Q_{\mathrm{Pei}} + c_9 E^{\alpha}_{\mathrm{GB}} \tag{10}$$

$$\tau^{\alpha'}_{\mathrm{Pei}} = \frac{Q_{\mathrm{eff}}}{c_3 b^3} \tag{11}$$

where c_9 is a fitting parameter, and E^{α}_{GB} is the activation energy for the penetration of a grain boundary by a mobile dislocation with the length b. For a detailed derivation of E^{α}_{GB} we refer to [7,13].

2.3. Evolution of the immobile dislocation densities

There are four processes contributing to the evolution of the statistically stored dislocation. The lock formation mechanism between mobile dislocations and forest dislocations, and the dipole mechanism between mobile dislocations with anti-parallel Burgers vector determine the multiplication terms, while the athermal annihilation of two parallel dislocations with anti-parallel Burgers vector within a critical distance and the thermal annihilation determine the annihilation terms. The complete rate equation system for the immobile SSD combines these four processes. For the details of these rate equations, we refer to Ma and Roters [9]. The only modification in this work is, that we assume thermal annihilation by cross slip of screw dislocations instead of climb of edge dislocations, so that the bulk diffusion activation energy Q_{bulk} has been replaced by Q_{cross}.

When orientation gradients are present in a volume portion geometrically necessary dislocations must be introduced to preserve the continuity of the lattice. Here we use the same equations for the evolution of this kind of dislocation as given in [9].

3. Channel die test of a Nb bicrystal

For the numerical simulation, we use plane strain compression to approximate the boundary condition of the

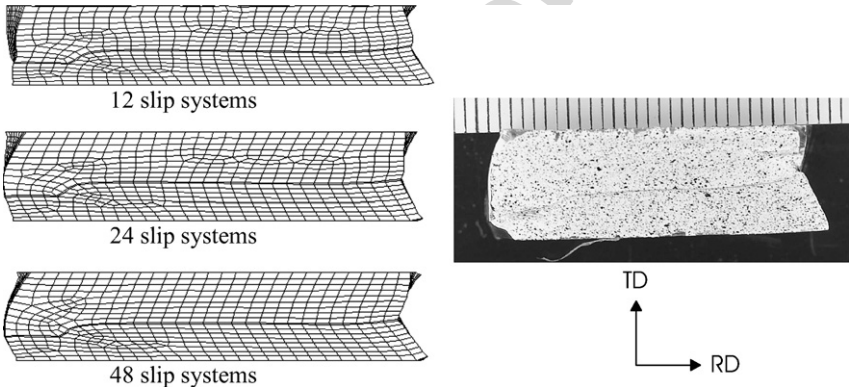

Fig. 2. Comparison of the sample shape after plane strain compression of about 40% for an Nb bicrystal for CP-FEM simulations using different slip system combinations and the experiment. The 12 slip systems are those in the $\langle 111\rangle\{110\}$ group, 24 slip systems are those in the $\langle 111\rangle\{110\}$ and the $\langle 111\rangle\{112\}$ groups, and 48 slip systems are those in the $\langle 111\rangle\{110\}$, the $\langle 111\rangle\{112\}$ and the $\langle 111\rangle\{123\}$ groups.

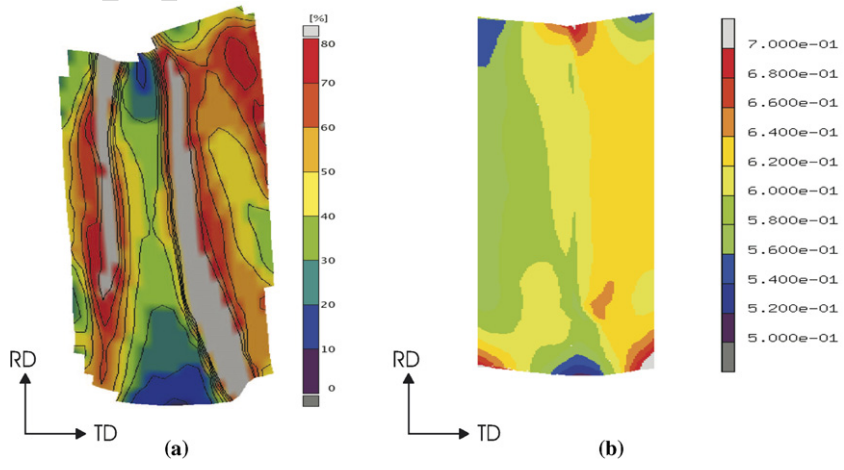

Fig. 3. Comparison of von Mises strain distribution for an Nb bicrystal: (a) is the experimental result measured by a digital image correlation technique after 38% compression and; (b) the calculated distribution.

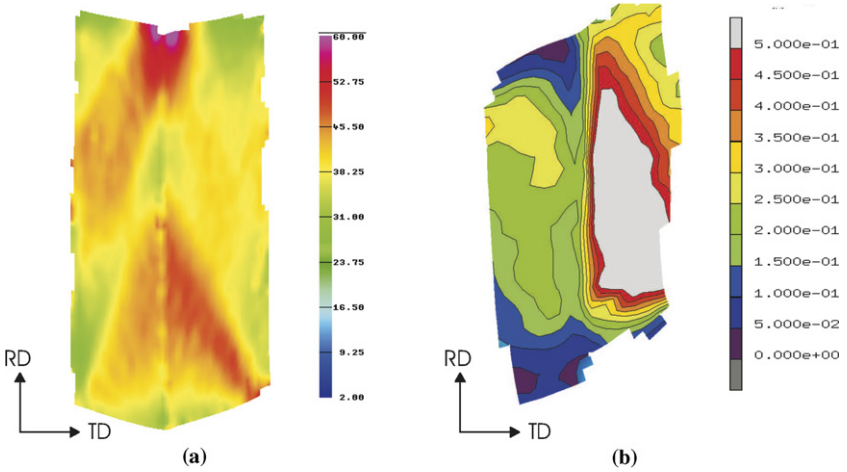

Fig. 4. Measured distribution of von Mises strain for an aluminium bicrystal with 17° misorientation: (a) after 40% compression and; (b) after 50% shear deformation [14].

channel die test. The orientation data obtained from the micro-texture measurements are expressed as $(\varphi_1,\Phi,\varphi_2)$ in Bunge–Euler notation in the coordinate system by rolling, transverse, and normal directions. For the finite element analysis the global coordinate system was defined by X parallel to RD, Y parallel to TD and Z parallel to ND. This means that the measured initial orientations could be directly assigned to the respective integration points.

From the literature several difficulties to distinguish which slip system is activated during the plastic deformation for BCC crystalline materials are reported [1]: TEM is not always able to distinguish exactly which slip system is activated; TEM investigations do not provide statistically reliable information since a very small volume of the specimen is examined; samples are always studied in an unloaded state; and the criterion for selecting active slip systems in polycrystalline aggregates is different from that for single crystals.

In order to determine which slip systems are activated during the channel die test of Nb bicrystals, in this paper, three combinations of slip systems are used in the simulation. The calculated sample shapes are compared with the experimental one in Fig. 2. It can be clearly seen, that the combination of $\langle 1\,1\,1\rangle\{1\,1\,0\}$ and $\langle 1\,1\,1\rangle\{1\,1\,2\}$ gives the best agreement. Therefore we conclude that at room temperature the plastic deformation of the Nb bicrystal is accommodated by 24 slip systems.

Using the combination of $\langle 1\,1\,1\rangle\{1\,1\,0\}$ and $\langle 1\,1\,1\rangle\{1\,1\,2\}$ slip systems, we compare the calculated Von Mises equivalent strain with the experimentally measured one on the TD–RD sample surface in Fig. 3. Both the experimental and simulation results show a larger plastic deformation in the right grain, which is caused by a larger Schmid factor or smaller Taylor factor. In the experiment there exist two strong deformation bands, one across the left crystal and one almost along the grain boundary line, which do not appear in the simulation.

In Fig. 4 we show two experimental results for a channel die test and a simple shear test for an Al bicrystal to compare the deformation behavior with that of Nb. One can see clearly, that compared to the bulk material the grain boundary zone behaves as a harder region for the Al bicrystal in both tests (Fig. 4) but like a softer region for the Nb bicrystal (Fig. 3).

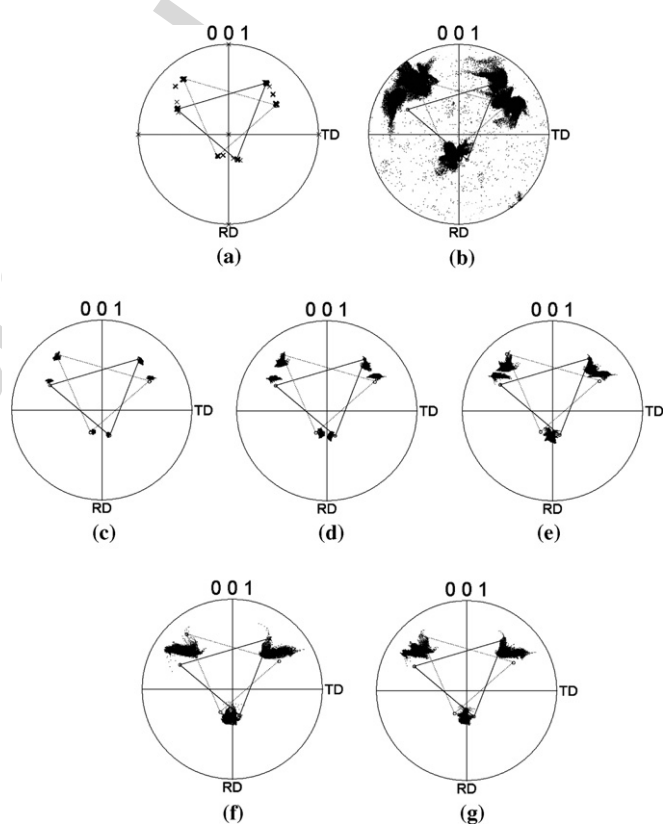

Fig. 5. Comparison of pole figures for an Nb bicrystal: (a) the measured initial pole figure, (b) the measured pole figure after 38% compression; (c–g) simulated pole figures for 8%, 16%, 24%, 32% and 40% compression, respectively. For every pole figure, the two initial orientations of the bicrystal used in the simulations are highlighted.

From the measured initial pole figure plot ((a) in Fig. 5), it can be seen, that the Nb sample is not a perfect bicrystal

before the deformation. After 38% reduction the experimental pole figure shows a very strong orientation dispersion compared with the simulated one ((b) and (g) in Fig. 5). From this comparison we can see that the model underestimates the texture spread for the BCC crystal.

4. Conclusions

From the comparison of the deformed sample shape we conclude, that a combination of $\langle 1\,1\,1\rangle\{1\,1\,0\}$ and $\langle 1\,1\,1\rangle\{1\,1\,2\}$ slip systems is mainly activated for the plastic deformation of the Nb bicrystal at room temperature.

Comparison with results for Al shows several differences for the grain boundary behavior and texture evolution between the FCC and the BCC bicrystals. However, the experimental conditions were quite different as well; the surface of the Nb sample shows grooves near the end of the two deformation bands. From the initial pole figure, it is clear that the sample is not a perfect bicrystal but has some orientation spread. Moreover, the grain boundary is neither horizontal nor flat. All these details are not sufficiently incorporated into the simulations. However, at the time being we only have experimental data from this single channel die test for the Nb bicrystal. Therefore, the reason for the deviations between the two sets of experiments (FCC and BCC) and between experiment and simulation (BCC) can not be clearly identified.

In the future several other Nb crystals of increasingly complex microstructure (i.e. with two grains, one triple junction, double triple junction, one grain surrounded by several other grains) will be deformed by channel die tests and simple shear tests to study the grain boundary effect in more detail in order to investigate the new model for BCC crystals.

References

[1] D. Raabe, Materials Science and Engineering A 197 (1995) 31–37.
[2] B. Sesták, A. Seeger, Zeitschrift für Metallkunde 69 (1978) 195–202.
[3] B. Sesták, A. Seeger, Zeitschrift für Metallkunde 69 (1978) 355–363.
[4] B. Sesták, A. Seeger, Zeitschrift für Metallkunde 69 (1978) 425–432.
[5] J.L. Raphanel, P. Van Houtte, Acta Metallurgica 33 (1985) 1481–1488.
[6] A. Ma, F. Roters, D. Raabe, Acta Materialia 54 (2006) 2169–2179.
[7] A. Ma, F. Roters, D. Raabe, Acta Materialia 54 (2006) 2181–2194.
[8] M. Sachtleber, Z. Zhao, D. Raabe, Materials Science and Engineering A 336 (1–2) (2002) 81–87.
[9] A. Ma, F. Roters, Acta Materialia 52 (12) (2004) 3603–3612.
[10] S.R. Kalidindi, C.A. Bronkhorst, L. Anand, Journal of Mechanics and Physics of Solids 40 (1992) 537–569.
[11] F. Roters, Physica Status Solidi B 240 (1) (2003) 68–74.
[12] L.P. Evers, W.A.M. Brekelmans, M.G.D. Geers, Journal of the Mechanics and Physics of Solids 52 (10) (2004) 2379–2401.
[13] A. Ma, F. Roters, D. Raabe. International Journal of Solid and Structures, submitted for publication.
[14] J.-C. Kuo. Mikrostrukturmechanik von Bikristallen mit Kippkorngrenzen. Ph.D. thesis, RWTH Aachen, 2004.